Pergamon

Progress in Surface Science, Vol. 46, No. 1, pp. 1–38, 1994

0079-6816/94 $24.00 + .00

0079-6816(94)E0001-Z

# SURFACE AND INTERFACE STRESS EFFECTS IN THIN FILMS

ROBERT C. CAMMARATA

*Department of Materials Science and Engineering*
*The Johns Hopkins University*
*Baltimore, Maryland 21218 U.S.A.*

## Abstract

Surface and interface stresses in solids are defined and their role in the thermodynamics of solids is presented. A discussion concerning the physical meaning of these quantities is given, along with a review of selected theoretical calculations and experimental measurements. It is shown that for a solid phase with one or more of its dimensions smaller than about 10 nm, the surface and interface stresses can be principal factors in determining the equilibrium structure and behavior of the solid. In particular, the effects of surface and interface stresses on thin films are reviewed along with the related topic of surface reconstructions in metals.

## Contents

## 1. Introduction

The thermodynamics of surfaces as formulated by Gibbs [1] has proven to be one of the most useful and powerful frameworks for studying surface phenomena. Central to this approach is the quantity referred to as the surface free energy. It is equal to the reversible work per unit area needed to create a surface and is the fundamental parameter that determines the behavior of fluid-fluid interfaces. However, when dealing with solid-fluid interfaces, there is another type of fundamental parameter, called the surface stress, that can also critically affect the behavior of surfaces. The surface stress is the reversible work per unit area needed to elastically stretch a pre-existing surface. Despite the extensive discussion surface stress has received over the years [2-7], there remains a great deal of confusion ' ing its meaning and importance.

As with the solid-fluid interface, there is a stress associated with the solid-solid interface. Actually, a general interface has associated with it two interface stresses corresponding to the two solid phases that are separated by the interface. An example of such an interface is the one between a thin film and a substrate. One of the interface stresses can be associated with work needed to stretch the film without straining the substrate. In this way the structure of the interface (for example, the density of misfit dislocations) can be changed. The other interface stress can be associated with the work to stretch both the film and substrate equally.

## 2. Surface Stress

### A. Thermodynamics of Surface Stress

In the Gibbsian formulation of the thermodynamics of surfaces [1], there is a quantity $\gamma$ that represents the excess free energy per unit area owing to the existence of a surface. It can also be considered the reversible work per unit area needed to create a new surface. In the case of a solid, this new area can be created by a process such as cleavage. The amount of reversible work dw performed to create new area dA of surface can be expressed as

$$dw = \gamma\, dA. \tag{1}$$

The total work needed to create a planar surface of area A (equivalently, the total excess free energy of the surface) is equal to $\gamma A$.

Gibbs [1] was the first to point out that for solids, there is another type of surface quantity, different from $\gamma$, that is associated with the reversible work per unit area needed

to elastically stretch a pre-existing surface. The relationship between this quantity and $\gamma$ can be derived in the following manner. The elastic deformation of a solid surface can be expressed in terms of a surface elastic strain tensor $\varepsilon_{ij}$, where i,j = 1,2. Consider a reversible process that causes a small variation in the area through an infinitesimal elastic strain $d\varepsilon_{ij}$. One can define a surface stress tensor $f_{ij}$ that relates the work associated with the variation in $\gamma A$, the total excess free energy of the surface, owing to the strain $d\varepsilon_{ij}$ (summing over each repeated index):

$$d(\gamma A) = A\, f_{ij}\, d\varepsilon_{ij}. \tag{2}$$

Equation (2) was first given by Shuttleworth [2], who derived it by considering the two reversible paths illustrated in Fig. 1. In the first path (clockwise), the solid pictured in the upper left is cleaved into two pieces and then both pieces are subjected to the same elastic strain. The work associated with the first step is $W_1 = 2\gamma_o A_o$, where $\gamma_o$ and $A_o$ are the excess surface free energy and area of each of the newly created (unstrained) surfaces. The work of the second step, denoted by $w_2$, equals the work needed to elastically deform the total bulk volume and the four (two original and two newly formed) surfaces. In the second path of Fig. 1 (counter-clockwise), the solid is first subjected to the elastic strain and is then cleaved into two pieces. The work of the first step, $w_1$, is equal to that needed to deform the bulk volume and the two surfaces. The difference $w_2 - w_1$ is equal to the excess work needed to elastically deform two surfaces of area $A_o$ to area $A(\varepsilon_{ij})$. This difference can be equated with the work performed against the surface stress $f_{ij}$:

$$w_2 - w_1 = 2 \int f_{ij}\, dA(\varepsilon_{ij}) = 2 \int A\, f_{ij}\, d\varepsilon_{ij}. \tag{3}$$

The work associated with the second step of the second path can be expressed as $W_2 = 2\,\gamma(\varepsilon_{ij})\, A(\varepsilon_{ij})$, so that $W_2 - W_1 = 2[\gamma(\varepsilon_{ij})A(\varepsilon_{ij}) - \gamma_o A_o]$. Equating the total works of the two reversible paths leads to $W_2 - W_1 = w_2 - w_1$. Therefore,

$$2[\gamma(\varepsilon_{ij})A(\varepsilon_{ij}) - \gamma_o A_o] = 2 \int A\, f_{ij}\, d\varepsilon_{ij}, \tag{4}$$

which is equivalent to Equation (2). Since $d(\gamma A) = \gamma\, dA + A\, d\gamma$, and $dA = A\, \delta_{ij}\, d\varepsilon_{ij}$ (where $\delta_{ij}$ is the Kronecker delta), the surface stress can be expressed as

$$f_{ij} = \gamma \delta_{ij} + \partial\gamma/\partial\varepsilon_{ij}. \tag{5}$$

In contrast to the excess surface free energy $\gamma$, which is a scalar, the surface stress $f_{ij}$ is a second rank tensor. For a general surface, it can be referred to a set of principal axes

such that the off-diagonal components are identically zero. Furthermore, the diagonal components are equal for a surface possessing a three-fold or higher rotation axis symmetry. This means that the surface stress for high symmetry surfaces is isotropic and can be taken as a scalar $f = \gamma + \partial\gamma/\partial\varepsilon$. Rewriting this as

$$f - \gamma = \partial\gamma/\partial\varepsilon \tag{6}$$

shows that the difference between the surface stress f and the surface free energy $\gamma$ is equal to the change in surface free energy per unit change in elastic strain of the surface. For most solids, $\partial\gamma/\partial\varepsilon \neq 0$; in fact, $\partial\gamma/\partial\varepsilon$ is usually the same order of magnitude as $\gamma$ and can be positive or negative, while $\gamma$ (for a clean surface) is always positive. Thus, f is also generally the same order of magnitude as $\gamma$ and can be positive or negative.

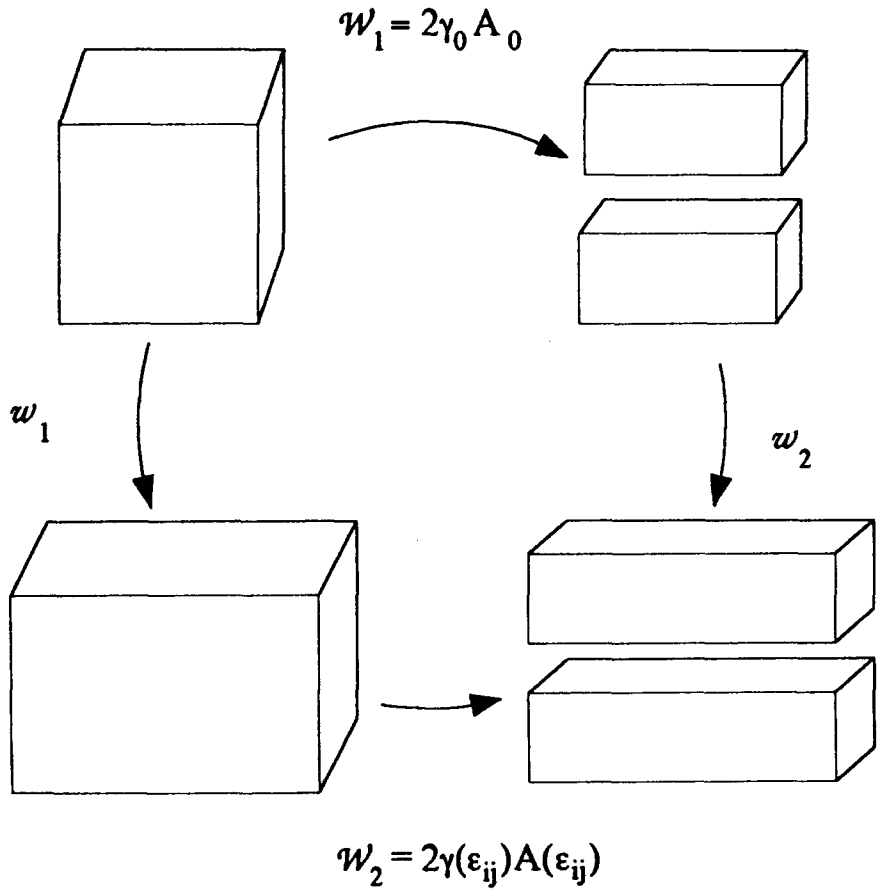


Figure 1. Schematic representation of two reversible paths that illustrate the relationship between surface free energy and surface stress.

Both f and $\gamma$ can each be considered as representing a force per unit length, the former exerted by a surface during elastic deformation, and the latter exerted by a surface during plastic deformation. As a result, both f and $\gamma$ have been referred to as "surface tension." This has undoubtedly contributed to some of the confusion in the literature concerning the difference between them, and it is probably best not to use the term when discussing solid surfaces.

It is often stated that, in contrast to solids, f and $\gamma$ are the same for fluids. This is due to the fact that when a fluid such as a soap film is stretched, the atoms or molecules in the interior move to the surface toaccommodate the new area created. In this case $\gamma$ remains constant during the stretching process, and according to Equation (6), $f = \gamma$. This has led some to claim by the same reasoning that at high temperatures where there is sufficient atomic mobility, $f = \gamma$ for solids during processes such as creep. However, this is not correct. During the initial elastic deformation in a creep experiment the work per unit area needed to stretch the solid is f, while during plastic deformation $\gamma$ represents the specific surface work to create new surface. Thus, the quantity being measured in a creep test, where the plastic strain is much greater than the elastic strain, is the surface free energy and not the surface stress.

For many processes, the easiest and most unambiguous way of determining whether f or $\gamma$ is the relevant parameter is the following: if a small variation in area does not change the surface atomic density, then the specific surface work is equal to $\gamma$; if the variation is due to an elastic strain that changes the surface density of atoms, then the specific surface work is f. According to this rule, plastic deformation and crack propagation are examples of processes where $\gamma$ equals the surface work, independent of mechanism. On the other hand (as is discussed in more detail later), the Laplace pressure associated with a small solid particle in a fluid is proportional to f. In the case of liquids, all processes of interest involve variations in area without varying the surface density, and the surface work represents a surface free energy. (However, in the case of a compressible liquid, it is possible to conceive of a surface stress-like quantity that represents the surface work when a liquid is subjected to a hydrostatic pressure.)

**B. Physical Origin of Surface Stress**

The physical origin of the surface stress can be qualitatively understood in the following manner. The nature of the chemical bonding (e.g., the number of bonds) of atoms at the surface is different from the bonding of atoms in the interior. Because of this, the surface atoms would have an equilibrium interatomic distance different from that of the interior atoms if the surface atoms were not constrained to remain structurally coherent with the underlying lattice. As a result, the interior of the solid can be considered as exerting a stress on the surface. There has been some confusion with regard to identifying

a surface stress of either sign as compressive or tensile. When f is positive, the surface work f dA is negative if dA is negative. This indicates that the surface could lower its energy by contracting and is therefore under tension. Therefore, a positive f is referred to as a tensile surface stress, while a negative f is referred to as a compressive surface stress.

A simple two-body interatomic force model to illustrate the origin of the surface stress was given by Shaler [8]. Consider an atom P in the interior of a face centered cubic crystal as shown in Fig. 2. The x and y axes are along the [100] and [010] directions. Attention is restricted to first and second nearest neighbor interactions. Let $a$ equal the force each nearest neighbor A atom exerts on P and $b$ equal the force exerted by each second nearest neighbor B atom. If the solid is in equilibrium, $a$ represents a force of repulsion and $b$ a force of attraction. A simple balance of forces requires that $b = -2\sqrt{2}a$. Now let the crystal be cleaved to create a (100) oriented surface containing the P atom. The force acting on the P atom in the y-direction is now $b + 3a/\sqrt{2} = -a/\sqrt{2}$. Since $a$ is a force of repulsion, the surface atoms are subjected to a net force in tension in the [010] direction. A similar calculation for atoms on a (111) oriented surface leads to a net compressive force of $+a$ along the $<1\bar{1}0>$ directions. It is interesting to note that this simple two-body central force model will lead to the result that f = 0 if only nearest neighbor interactions are considered [6], and that in order to get a nonzero surface stress, at least second nearest neighbor interactions must be taken into account.

As discussed by Needs et al. [9], the loss of neighbors which results from the creation of a metal surface reduces the local electron density around the atoms near the surface. Since the surface atoms now sit in a lower average charge density than the optimal value associated with the bulk atoms, the response of the surface atoms would presumably be to attempt to reduce their interatomic distances in order to increase the average electron density. Such surfaces would therefore be expected to display a positive surface stress. Theoretical and experimental results seem to support this conclusion, at least for ideal 1 x 1 low index surfaces. If the surface stress (actually, the difference between the surface stress and the surface free energy) is large enough, it will be thermodynamically more favorable for the surface layer to contract so that the surface atoms are no longer in perfect registry with the underlying lattice. This type of surface reconstruction has been observed for (111) oriented surfaces of Au and Pt (see Section 4).

### C. Lagrangian Coordinate System

Referring back to Equation (5), the first term on the right hand side takes into account the change in area due to the elastic deformation, while the second term accounts for the change in surface free energy with elastic strain. As pointed out by Cahn [7,10], the expression for the surface stress can be simplified by using a Lagrangian measure of the area. The relation between the Lagrangian area $A_L$ and the physical area A is

$$A = A_L(1 + \varepsilon_{ii}), \tag{7}$$

where $\varepsilon_{ii}$ represents the trace of the elastic strain $\varepsilon_{ij}$. $A_L$ is the surface area measured with respect to a standard state of strain, and remains unchanged during elastic deformation. In the Lagrangian coordinate system, it is necessary to define the surface free energy $\gamma_L$ such that $\gamma_L A_L = \gamma A$:

$$\gamma_L = \gamma(1 + \varepsilon_{ii}). \tag{8}$$

The two types of surface work that can be performed on a solid to change its physical area A can be taken as either (a) changing $A_L$ holding $\varepsilon_{ij}$ constant, or (b) changing $\varepsilon_{ij}$ holding $A_L$ constant. The former surface work is equal to the surface free energy $\gamma_L$, while the latter surface work is equal to the surface stress which can be expressed as

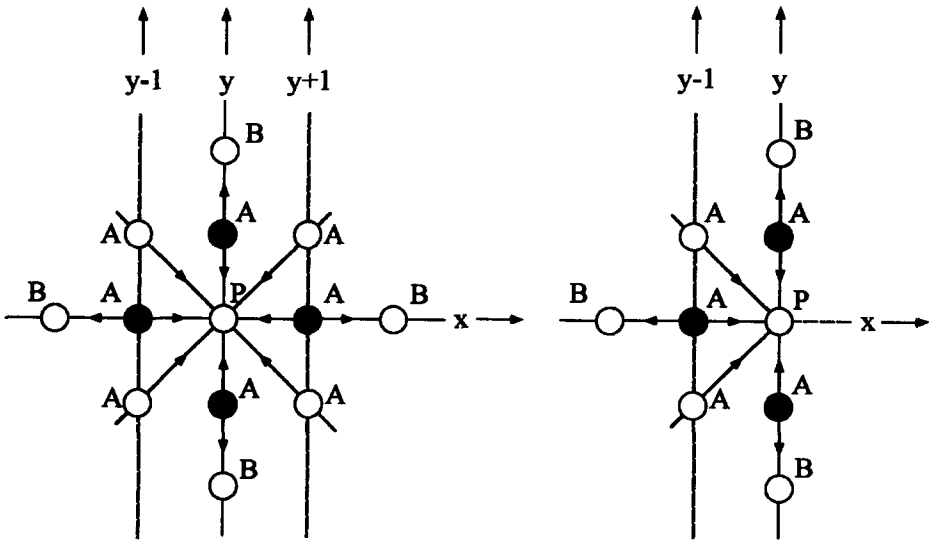


Figure 2. Illustration of how interatomic forces acting on surface atoms can result in a surface stress [8].

$$f_{ij} = \partial\gamma_L/\partial\varepsilon_{ij}. \tag{9}$$

Substituting Equation (8) into Equation (9) leads to Equation (5). For many problems, the use of the Lagrangian coordinate system greatly simplifies the analysis.

**D. Equilibrium of a Small Solid Crystal**

Consider a fluid (liquid or vapor) droplet in equilibrium with a different surrounding fluid that can be considered infinite in extent. There will be a pressure difference $\Delta P = P_1 - P_2$ (where the subscripts 1 and 2 refer to the droplet and the surrounding fluid, respectively) acting on the droplet owing to the surface free energy. At equilibrium, the virtual work $\Delta P\, dV$ resulting from a small variation in the volume of the droplet due to transfer of atoms or molecules from the surrounding fluid to the droplet will equal $\gamma\, dA$, the increase in the total free energy of the surface. For a spherical droplet of radius r, this equality leads to the well known Laplace–Young Equation:

$$\Delta P = 2\gamma/r. \tag{10}$$

Because of this Laplace pressure $\Delta P$, the chemical potential $\mu$ of the droplet phase will contain a term $2\gamma V/r$, where V is the molar volume of the droplet phase. At equilibrium, the chemical potential of the surrounding fluid phase will also contain this term, and the chemical potentials of the two phases will be equal.

Now consider the case of a small single component solid crystal in equilibrium with a surrounding fluid. For simplicity, it will be assumed that the solid is spherical and has an isotropic surface stress f. The surface stress exerts a hydrostatic pressure equal to $2f/r$ that when added to the pressure of the fluid is equal to the pressure of the solid. Thus, the Laplace pressure $\Delta P = P_s - P_f$ (where the subscripts s and f denote solid and fluid, respectively) for a solid is expressed as

$$\Delta P = 2f/r. \tag{11}$$

In the literature, the Laplace pressure for a solid is often incorrectly written as Equation (10) rather than as Equation (11).

As discussed by Gibbs [1], and more recently by Cahn [10], the chemical potential of the solid phase will contain the term $2fV/r$, where V is the molar volume of the solid. This is because a transfer of material from the fluid to the solid phase will change the Laplace pressure acting on the solid. However, the chemical potential of the fluid phase will

contain the term $2\gamma V/r$, reflecting the fact that the transfer changes the physical area of the solid-fluid interface. This leads to the result

$$\mu_s - \mu_f = 2(f - \gamma)V/r. \tag{12}$$

(Gibbs pointed out that Equation (12) is strictly true only for the case of an incompressible solid; because of the small compressibility of most solids, correction terms will in general be negligible [1].) It is to be noted that, except for the special case of $f = \gamma$, the chemical potentials of the two phases in equilibrium are not the same. Gibbs restricted his attention to a single component solid in equilibrium with a multicomponent fluid. Cahn [10] extended the analysis for the case of a multicomponent solid with both substitutional and interstitial components. The analysis is simplified if the Lagrangian coordinate system is used. In the case of an interstitial component, the transfer of atoms from the fluid to the solid does not change the Lagrangian surface area but can induce an elastic strain if the component has a nonzero partial molar volume. Cahn showed that for interstitial components, the chemical potential is the same for solid and fluid phases ($\mu_s - \mu_f = 0$), while for the substitutional components the difference is given by Equation (12), where V is now the volume of the solid divided by the number of moles of substitutional lattices sites.

Examples of various thermodynamic derivations employing the correct expression for the Laplace pressure of the solid have been given by Cahn [10]. Some of his results are given below in order to illustrate under what circumstances the equilibrium behavior is determined by $\gamma_L$ and/or f. The Lagrangian measure of the surface free energy is used in order to emphasize the fact that in his derivations, Cahn used the Lagrangian coordinate system which significantly reduced the complexity of his analysis. The difference between the bulk melting temperature $T_m$ and the melting temperature T of a finite-sized single component solid is

$$T_m - T = 2\gamma_L V/r\,(S_l - S_s), \tag{13}$$

where $S_l$ and $S_s$ are the molar entropies of the liquid and solid, respectively. Since melting or freezing a surface layer of atoms changes the Lagrangian area, the relevant surface parameter is the surface free energy. Similarly, the solubility of a dilute single component solid in a multicomponent fluid is given by

$$c = c_o \exp(2\gamma_L V/rRT), \tag{13a}$$

where c is the concentration in the fluid for a particle of radius r, $c_o$ is the saturation concentration for large particles, R is the gas constant, and T is the absolute temperature.

Again, $\gamma_L$ is the appropriate parameter since dissolving a layer from the solid changes the Lagrangian area. The equilibrium vapor pressure P for a single component solid sphere of radius r, assuming the vapor is monatomic, can be expressed as

$$P = P_O \exp(2\gamma_L V/rRT), \tag{14}$$

where $P_O$ is the equilibrium vapor pressure for a solid with a large planar area. Since evaporation from the solid changes the Lagrangian area, the equilibrium vapor pressure depends on $\gamma_L$. Consideration is now given to the vapor pressure of a dilute interstitial component. Assuming the component vaporizes in monatomic form, the vapor pressure P is

$$P = P_O \exp(2f - V/rRT) \tag{15}$$

where $\bar{V}$ is the partial molar volume of the component in the solid. In this case, f is the appropriate parameter because transfer of interstitial component atoms does not change the Lagrangian area but does work against the surface stress if the component has a nonzero partial molar volume. As a final example, the vapor pressure of a dilute substitutional component that vaporizes in monatomic form can be expressed as

$$P = P_O \exp(2[\gamma_L V + f(V - \bar{V})]/rRT). \tag{16}$$

The term involving $\gamma_L$ accounts for the change in Lagrangian area, while the term involving f reflects the work performed against the surface stress when the partial molar volume of the substitutional component is different from V.

Many derivations in the literature do not employ the correct expression for the Laplace pressure of a solid, using $\gamma$ instead of f in Equation (11). As a result, they apply only for the special case of $f = \gamma$, which is rarely expected. Even though some derivations using the incorrect expression for the Laplace pressure for the solid can produce the correct result [as is often the case for many derivations of Equations (13) and (14)], it is obviously impossible to obtain Equations (15) and (16) without Considering effects of the surface stress.

**E. Theoretical Calculations**

Theoretical calculations of surface stresses generally involve calculating the surface free energy and its derivative with respect to elastic strain. Both first principles and atomistic potential calculations have been attempted. Though some molecular dynamics

simulations have been performed that give the variation of the surface stress with temperature (for example, see reference 11), the vast majority of results are obtained for a temperature of 0 K. It is to be noted that, except for the inert gas crystals, most of the surface stresses for low index surfaces of single component materials are positive and of the same order of magnitude as the surface free energy.

*(i) Inert Gas Crystals.* Calculations of the surface stress of inert gas crystals date back to the work of Shuttleworth [2]. His results suggested that for the (100) oriented surfaces of Ne, Ar, Kr, and Xe, the surface stresses were negative and about a factor of ten smaller in magnitude than the surface free energy.

*(ii) Metals.* First principle calculations for several clean fcc metal surfaces have been performed by Needs and coworkers [9,12-14] using a pseudopotential total energy technique that employed a local density approximation for the exchange-correlation energy. Values of the surface free energy and surface stress for unreconstructed fcc (111) oriented metal surfaces are given in Table 1. It is seen that all surfaces exhibit a tensile (positive) surface stress. In order to gain a greater understanding of the physical origin of the surface stress, Needs et al. [9] calculated the electrostatic, exchange-correlation, and kinetic energy contributions to the surface stress of Al(111). They found that the largest contributor was the term associated with the kinetic energy, while the other two terms were significantly smaller in magnitude and negative. A similar result was also obtained using a jellium model that had the same average electron density as aluminum. Needs et al. [9] state that the same general behavior should be expected for metals with relatively high electron densities. For metals with lower electron densities (for example, the alkali metals), it is expected that the electrostatic, exchange-correlation, and kinetic energy terms all contribute significantly to the value of the surface stress.

TABLE 1. First principles calculations of surface free energy $\gamma$ and surface stress f for clean unreconstructed (111) oriented fcc metal surfaces [12-14].

| Metal | $\gamma$ [J/m$^2$] | f [J/m$^2$] |
|---|---|---|
| Al | 0.96 | 1.25 |
| Ir | 3.26 | 5.30 |
| Pt | 2.19 | 5.60 |
| Au | 1.25 | 2.77 |
| Pb | 0.50 | 0.82 |

Calculations of the surface stress for various metals have been made using embedded atom method [15,16] and Finnis-Sinclair [17,18] potentials. Examples of the surface free energy and principal surface stresses for certain fcc [15] and bcc [17] metals are given in Table 2. A comparison of the values of $\gamma$ and f for (111) oriented surfaces of Au

TABLE 2. Calculated surface free energy $\gamma$ and principal surface stresses $f_{xx}$ and $f_{yy}$ for clean unreconstructed metal surfaces using embedded atom method potentials for the fcc metals [15] and Finnis-Sinclair potentials for the bcc metals [17]. Note: For bcc (110) surfaces, x = [1$\bar{1}$0], y = [001]; for bcc (310) surfaces, x = [1$\bar{3}$0], y = [001].

| Surface | $\gamma$ [J/m$^2$] | $f_{xx}$ [J/m$^2$] | $f_{yy}$ [J/m$^2$] |
|---|---|---|---|
| Ni (100) | 1.57 | 1.27 | |
| (111) | 1.44 | 0.43 | |
| Cu (100) | 1.29 | 1.38 | |
| (111) | 1.18 | 0.86 | |
| Ag (100) | 0.70 | 0.82 | |
| (111) | 0.62 | 0.64 | |
| Au (100) | 0.92 | 1.79 | |
| (111) | 0.79 | 1.51 | |
| Pt (100) | 1.64 | 2.69 | |
| (111) | 1.44 | 2.86 | |
| V (100) | 1.733 | 2.424 | |
| (110) | 1.473 | 1.939 | 0.263 |
| (310) | 1.745 | 2.335 | 1.255 |
| Nb (100) | 1.956 | 2.532 | |
| (110) | 1.669 | 2.168 | 0.301 |
| (310) | 2.104 | 2.405 | 1.267 |
| Ta (100) | 2.328 | 3.249 | |
| (110) | 1.980 | 2.535 | 0.392 |
| (310) | 2.512 | 3.085 | 1.647 |
| Mo (100) | 2.100 | 2.241 | |
| (110) | 1.829 | 2.019 | 0.775 |
| (310) | 2.070 | 2.247 | 1.184 |
| W (100) | 2.924 | 3.032 | |
| (110) | 2.575 | 2.385 | 0.271 |
| (310) | 3.036 | 2.833 | 1.450 |

and Pt given in Tables 1 and 2 shows that the values obtained using the semi-empirical potentials are significantly smaller than those obtained from the first principles calculations. Recently, modified embedded atom method potentials have been developed that yield values of the surface free energy and surface stress closer to the first principles values [19].

*(iii) Semiconductors.* First principles calculations, using the pseudopotential technique and employing a local density approximation, were performed by Meade and Vanderbilt [20,21] for elemental and chemisorbed (111) oriented surfaces of Si and Ge. Values of the surface free energy and the surface stress are listed in Table 3 and are given in units of eV per 1 x 1 cell. Meade and Vanderbilt analyzed various factors that affect the value of the surface stress and concluded that surface bonding topology, atomic size, and the chemical nature of the adsorbate species all make important contributions.

In the case of (111) surfaces of compounds such as GaAs and InSb, there is an A type surface, where the terminating plane is composed of Group III atoms, and a B type surface, where the terminating plane is composed of Group V atoms. By considering the geometry associated with the hybridization of the covalent bonds, Cahn and Hanneman [22] concluded that an A type surface should be under compression, while a B type surface should be under tension, with the magnitude of the B surface stress being somewhat less

TABLE 3. Calculated surface free energy $\gamma$ and surface stress f for Si(111) and Ge(111) surfaces [20,21]. Note: faulted = stacking fault at the surface.

| Surface | | $\gamma$ [eV/1 x 1 cell] | f [eV/1 x 1 cell] |
|---|---|---|---|
| Si | 1 x 1 | 1.45 | -0.54 |
| | 1 x 1 faulted | 1.51 | 0.11 |
| | $\sqrt{3} \times \sqrt{3}$ adatom | 1.27 | 1.70 |
| | 2 x 2 adatom | 1.24 | 1.66 |
| | 2 x 2 adatom-faulted | 1.27 | 1.89 |
| Si(Ga) | 1 x 1 | -3.01 | -4.45 |
| | $\sqrt{3} \times \sqrt{3}$ | -0.35 | 1.35 |
| Ge | 1 x 1 | 1.40 | -0.73 |
| | 1 x 1 faulted | 1.45 | -0.26 |
| | 2 x 2 adatom | 1.20 | 1.43 |
| | 2 x 2 adatom-faulted | 1.22 | 1.67 |

than that for the A surface. They performed a calculation based on the forces associated with the elastic distortion of the covalent bonds, which they estimated from the bulk elastic constants, in order to estimate the (111) surface stresses of various compounds (see Table 4).

TABLE 4. Calculated values of (111) surface stresses for A and B surfaces of III-V compounds [22].

| Material | $f_A$ [J/m$^2$] | $f_B$ [J/m$^2$] |
|---|---|---|
| InSb | - 0.6 | 0.3 |
| GaAs | - 1.0 | 0.5 |
| InAs | - 0.7 | 0.3 |
| GaSb | - 0.8 | 0.4 |
| AlSb | - 0.8 | 0.4 |

***(iv) Ionic Solids.*** Several attempts have been made over the years to calculate the surface stress of ionic solids [2,11,23-25]. The most commonly studied surface is the (100) oriented surface of alkali halides. It appears that the results of these calculations are very sensitive to the details of the calculation such as the type of structural relaxations that are allowed [11]. Early calculations by Shuttleworth [2] gave negative values for the surface stresses of several alkali halides, a result that appears to be due to the manner in which the surfaces were allowed to relax [11]. The current consensus is that most if not all of the (100) oriented alkali halide surfaces display a positive surface stress. Table 5 lists values of surface stress obtained by Nicholson [23].

**F. Experimental Measurements**

Stresses of all types are generally determined by measuring an elastic strain that results from that stress and then using the appropriate form of Hooke's Law to extract the stress value. This is also true for the majority of surface stress measurements. To illustrate how this can be performed, consider a small solid sphere of radius r that is presumed to have an isotropic surface stress f. According to Equation (11) the Laplace pressure acting on this sphere is equal to $\Delta P = 2f/r$. This will induce an elastic strain in the solid. Since this strain is in response to a hydrostatic pressure, the appropriate form of Hooke's Law, which is assumed to be valid for these small solids, is $-\Delta P = K\varepsilon_V = 3K\varepsilon$, where K is the bulk modulus, $\varepsilon_V$ is the volume strain, and $\varepsilon$ is the radial strain. The surface stress is computed by measuring the radial strain in a sphere of a known radius:

$$f = -3K\varepsilon r/2. \tag{17}$$

Vermaak and coworkers [26-28] measured the radial strain in small spheres of Au, Ag, and Pt by electron diffraction and determined an average surface stress using Equation (17). Their results are listed in Table 6. These values are within a factor of two or so of those obtained from the theoretical calculations for the low index surface stresses (at 0 K) found in Tables 1 and/or 2.

A thin rectangular wafer whose top and bottom surface have different surface stresses will bend in response to that difference. By measuring the radius of curvature R

TABLE 5. Calculated values of the surface stress f for (100) surfaces of alkali halides [23].

| Material | f [J/m$^2$] |
|---|---|
| LiF | 2.287 |
| LiCl | 1.025 |
| LiBr | 0.827 |
| LiI | 0.558 |
| NaF | 1.031 |
| NaCl | 0.562 |
| NaBr | 0.454 |
| NaI | 0.303 |
| KF | 0.549 |
| KCl | 0.310 |
| KBr | 0.250 |
| KI | 0.172 |
| RbF | 0.427 |
| RbCl | 0.248 |
| RbBr | 0.204 |
| RbI | 0.142 |
| CsF | 0.308 |

TABLE 6. Experimental measurements of surface stress [26-28].

| Material | f [J/m$^2$] | Temperature [$^o$C] |
|---|---|---|
| Au | $1.175 \pm 0.2$ | 50 |
| Ag | $1.415 \pm 0.3$ | 55 |
| Pt | $2.574 \pm 0.4$ | 65 |

of the bent wafer, the difference in the surface stresses of the two surfaces, $\Delta f$, can be calculated using the Stoney formula [22,29]

$$\Delta f = Yt^2/6R, \tag{18}$$

where t is the thickness of the wafer and Y is the appropriate elastic modulus. [For an isotropic solid, $Y = E/(1 - \nu)$, where E is Young's modulus and $\nu$ is Poisson's ratio.] When radius of curvature measurements of (111) oriented InSb wafers obtained by Hanneman et al. [30] were used in Equation (18), a value of $\Delta f$ of 0.95 to 1.4 $J/m^2$ was obtained [22]. This result is in good agreement with the difference in the calculated values for the A and B surfaces of InSb given in Table 4.

Recently, Martinez et al. [31] used the wafer bending technique to obtain the surface stress of the reconstructed 7 x 7 Si(111) surface. One third of a monolayer of Ga was deposited onto one side of a wafer with initially clean Si(111) 7 x 7 surfaces. The wafer was then heated until the Si(Ga) surface displayed a sharp transition to a $\sqrt{3} \times \sqrt{3}$ structure as determined by low energy electron diffraction. The wafer was observed to bend due to the difference in the surface stresses of the 7 x 7 and the $\sqrt{3} \times \sqrt{3}$ surfaces, and the measured surface stress difference was 1.02 eV/(1 x 1 cell). If the theoretical calculation of 1.35 eV/(1 x 1 cell) for the $\sqrt{3} \times \sqrt{3}$ Si(Ga) surface given in Table 3 is added to this difference, the absolute surface stress of the clean 7 x 7 surface is estimated to be about 2.37 eV/(1 x 1 cell). Similar experiments were performed by Schell-Sorokin and Tromp [31a] in order to measure the difference in the average surface stress between a clean Si(100) surface and one with adsorbed As or Ge. The measured value for the difference in the surface stresses of 2 x 1 Si and 2 x 1 Si(As) surfaces of 1.2 eV/(1 x 1 cell) was in reasonable agreement with theoretical calculation [31b].

Anomalies in the dispersion behavior of surface phonons of Ni(110) have been attributed to surface stress effects [32]. From an analysis of the surface phonon spectra, surface stress values of 4.2 $J/m^2$ and 2.1 $J/m^2$ were determined for the [001] and [$1\bar{1}0$] directions, respectively.

## 3. Interface Stress

As with the solid-vapor and solid-liquid interfaces, there is a stress associated with a solid-solid interface. In fact, as pointed out by Brooks [4], a general interface has associated with it two interface stresses corresponding to the two solid phases that are separated by the interface. Following Cahn and Larché [33], one can define an interface stress $g_{ij}$ corresponding to the reversible work per unit area needed to strain one of the phases relative to the other, and another interface stress $h_{ij}$ associated with the reversible work per

unit area needed to equally stretch both phases. As with the case of a free solid surface, there are different ways of defining the area of the interface. In the general case where both types of strains are possible, there is some advantage to using a Lagrangian coordinate system (see Section 2). Consider two phases 1 and 2 separated by an initially coherent interface. Let $\varepsilon_{ij}$ denote the strain resulting from deforming phase 2 relative to phase 1, where $\varepsilon_{ij} = 0$ represents a lattice-matched interface. A second strain $e_{ij}$ is defined as that resulting from equally stretching both phases. Using the Lagrangian area of phase 1 as the reference area, and letting $\sigma_L$ represent the interfacial free energy measured in this Lagrangian coordinate system, the surface stresses can be defined as

$$g_{ij} = \partial\sigma_L/\partial\varepsilon_{ij}, \tag{19}$$

and

$$h_{ij} = \partial\sigma_L/\partial e_{ij}. \tag{20}$$

The interfacial free energy $\sigma_L(\varepsilon_{ij},e_{ij})$ for a general state of strain and interface structure can be expressed up to first order in the strains as

$$\sigma_L(\varepsilon_{ij},e_{ij}) = \sigma_L(0,0) + g_{ij}\varepsilon_{ij} + h_{ij}e_{ij}. \tag{21}$$

Consider a small spherical solid inclusion denoted as phase 2 embedded in an infinite solid matrix denoted as phase 1 (whose Lagrangian area is taken as the reference area). It will be assumed that the phases and the interface stresses g and h are isotropic. Let the reference states for the two phases be their respective stress-free states at zero pressure. Suppose that in these states the inclusion would have a radius $r_2$ and the matrix a hole of radius $r_1$ with $r_2 = (1 + \varepsilon)r_1$. Cahn and Larché [33] have shown that at equilibrium the true physical radius r of the hole is

$$r = r_1 + M(r_1\varepsilon - 2h/3K_2), \tag{22}$$

and the pressure in the inclusion is

$$P = M(2h/r_1 + 4G_1\varepsilon), \tag{23}$$

where $G_1$ is the shear modulus of the matrix, $K_2$ is the bulk modulus of the inclusion, and M is an elastic accommodation factor equal to $3K_2/(4G_1 + 3K_2)$. The factor M can range

from 0, when $K_2 = 0$ (corresponding to a void) and $P = 0$, to 1, when $G_1 = 0$ (corresponding to a liquid) and $P = 2h/r_1$, analogous to Equation (11). For intermediate values of M, the pressure P is composed of two terms: one reflecting the effect of the surface stress h and the other reflecting the fact that, in contrast to the case of a particle in a fluid, the matrix can sustain a shear stress. As was the situation for equilibrium of a small solid immersed in an infinite fluid, the chemical potentials of phases 1 and 2 are not equal. For example, suppose that phase 1 is composed of a single component $i$ that has precipitated from a binary phase (phase 2). The difference in the chemical potentials of $i$ between the two phases is (ignoring higher order strain energy terms that are small)

$$\mu_1 - \mu_2 = (P - 2\sigma_L/r_1)V, \tag{24}$$

where V is the stress-free molar volume of phase 1 [33].

Although the formulation of interface stresses given by Cahn and Larché is useful for many types of problems (for example, the thermodynamics of solid state nucleation [33]), a somewhat different approach will be given below that will facilitate the discussion of interface stress effects in thin films as given in Section 4.

**A. Interface Stress Associated with Stretching One Phase Relative to the Other**

For an interface between two crystals, the strain associated with the interface stress g results in a change of the interface structure. As an example, consider an epitaxial thin film on a semi-infinite rigid substrate. Changing the misfit dislocation density at the interface allows the lattice parameter of the film to be varied while keeping the lattice parameter of the substrate fixed. The interface stress g can be interpreted as the specific surface work associated with changing the dislocation density. In order to illustrate this, consider as the reference state a noncoherent interface where both the film and substrate have their bulk lattice parameters. Let $\varepsilon_m$ be defined as the misfit strain equal to $(a_s - a_f)/a_f$, where $a_s$ and $a_f$ are the bulk lattice parameters of the substrate and film, respectively, and let $\varepsilon$ represent the in-plane strain of the film measured with respect to its bulk state. (Note that this strain is different from the strain $\varepsilon$ defined using the Cahn-Larché formalism). When the film is strained by an amount $\varepsilon$, the strain that needs to be accommodated by misfit dislocations is $(\varepsilon_m - \varepsilon)$. For simplicity, it will be assumed that the misfit dislocations are edge dislocations with their Burgers vectors in the plane of the interface and are arranged in a square grid. The interface energy per unit area $\sigma$ of this dislocation grid can be expressed as [34]

$$\sigma = \sigma_0[1 - (\varepsilon_{11} + \varepsilon_{22})/2\varepsilon_m], \tag{25}$$

where the strain components $\varepsilon_{11} = \varepsilon_{22} = \varepsilon$, and

$$\sigma_o = Cb \mid \varepsilon_m \mid [ln(t/b) + 1]/2\pi. \tag{26}$$

In Equation (26), b is the magnitude of the Burgers vector, t is the film thickness, and C is an effective elastic modulus equal to $2[(1 - \nu_f)/G_f + (1 - \nu_s)/G_s]^{-1}$, where $\nu_f$ and $\nu_s$ are Poisson's ratio of the film and substrate, and $G_f$ and $G_s$ are the shear moduli of the film and substrate.

Taking the interface stress g as the work per unit physical area associated with introducing a strain $\varepsilon_{11}$ holding $\varepsilon_{22}$ constant in a film initially with $\varepsilon_{11} = \varepsilon_{22} = 0$ leads to

$$g = \sigma_o - (\partial\sigma/\partial\varepsilon_{11}) \mid_{\varepsilon_{11} = \varepsilon_{22} = 0} = \sigma_o [1 - 1/(2\varepsilon_m)]. \tag{27}$$

Defined in this way, the change in interfacial free energy $\Delta\sigma$ due to the introduction of a coherency strain $\varepsilon_{11}$ in an initially noncoherent interface is

$$\Delta\sigma = (g - \sigma_o)\varepsilon_{11}. \tag{28}$$

**B. Interface Stress Associated with Stretching Both Phases Equally**

In the very few theoretical or experimental studies that have been performed to investigate interface stresses, virtually all have been devoted to measuring $h_{ij}$, the work per unit area needed to stretch an interface by elastically straining both phases on each side of that interface by the same amount $e_{ij}$. Proceeding in a manner analogous to that used to derive Equation (5), this stress can be related to the interfacial free energy $\sigma$ by

$$h_{ij} = \sigma\,\delta_{ij} + \partial\sigma/\partial e_{ij}. \tag{29}$$

In Equation (29), $h_{ij}$ is the work per unit of actual physical area of interface as it changes with strain. Gumbsch and Daw [15] have calculated values for this type of interface stress for (100) and (111) metal-metal interfaces using standard embedded atom method potentials. Their results are given in Table 7. As was discussed in Section 2, calculations for free solid surfaces using embedded atom method potentials can significantly underestimate values of surface properties compared to those obtained from first principles calculations. Recently, embedded atom method potentials have been modified so that they give values for the free surface properties approximately equal to those obtained by first principles calculations [19]. These potentials were then used to evaluate interface stresses. For the case of a noncoherent Ag-Ni (111) interface, a value of $1.32\,J/m^2$ was obtained which is significantly larger than the value given in Table 7. However, both values are of opposite sign to that measured by experiment (see below).

A few attempts have been made to experimentally measure the interface stress h in layered materials. Crystalline polymers and organic crystals have a lamellar structure and display variations in their lattice parameters that are inversely proportional with lamella thickness. This behavior can be attributed to the effects of an interface stress [35]. The physical origin of this interface stress in crystalline polymers can be understood in the following manner. Figure 3 schematically shows a chain folded molecule in a lamella of a crystalline polymer. For a thick lamella with very long stem lengths, the stems have an equilibrium separation determined by the balance of van der Waals attractive forces and intermolecular repulsive forces. The chain folds are high energy configurations that would attempt to straighten out if they were not constrained by the stems. Thus, the chain folds at the interface can be considered under compression, and the interfaces therefore display a negative interface stress.

The manner in which the interface stress $h_{ij}$ can be obtained by lattice parameter measurements is now given [35]. The virtual work dw resulting from a variation in elastic strain $de_{ij}$ of a lamella is

$$dw = A(ts_{ij} + h_{ij})\, de_{ij}, \tag{30}$$

where t is the lamella thickness and $s_{ij}$ is the volume elastic stress. At equilibrium, dw = 0, so that

$$h_{ij} = - t\, s_{ij} = - t\, C_{ijkl}\, e_{kl}, \tag{31}$$

Table 7 Calculations of interface stress h for noncoherent metal-metal interfaces [15].

| Bilayer A/B | h for (100) interface [J/m$^2$] | h for (111) interface [J/m$^2$] |
|---|---|---|
| Ag/Ni | 0.83 | 0.32 |
| Au/Ni | 0.71 | -0.08 |
| Ag/Cu | 0.53 | 0.32 |
| Au/Cu | 0.33 | 0.01 |
| Pt/Ni | 0.04 | - 0.57 |

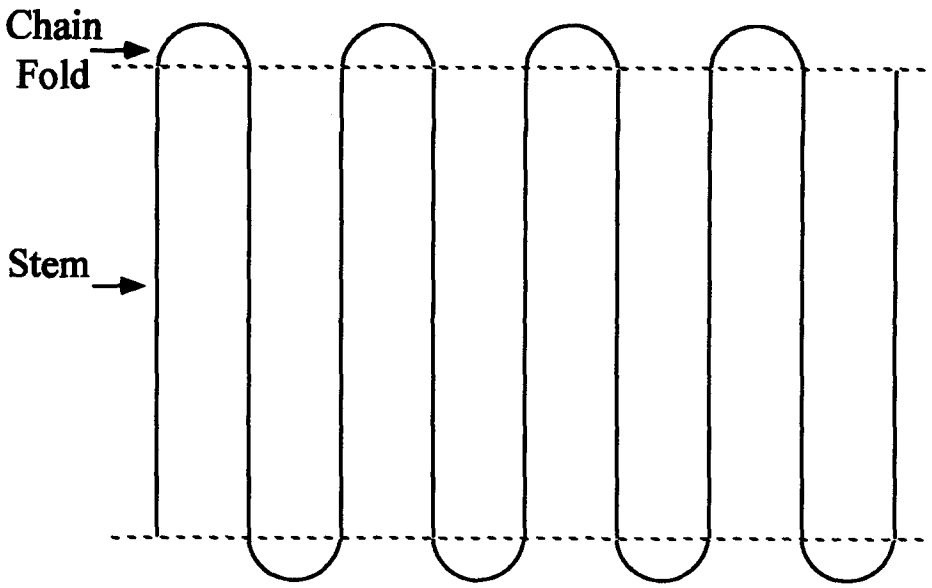


Figure 3. Schematic diagram of a molecule in a crystalline polymer lamella. The chain folds at the lamella interfaces lead to a compressive interface stress.

where $C_{ijkl}$ is the elastic stiffness tensor. Rearranging this so that strain is the dependent variable gives

$$e_{ij} = -S_{ijkl}\, h_{kl}/t, \tag{32}$$

where $S_{ijkl}$ is the elastic compliance tensor. The strain relative to an infinitely thick lamella should be proportional to the lamella thickness. This behavior has been observed in x-ray diffraction experiments of orthorhombic n-paraffins [36], melt crystallized and solution crystallized polyethylene [37], and crystalline random copolymers composed of tetrafluoroethylene and hexafluoropropylene [38].

In order to simplify the analysis, let the surface stress tensor $h_{ij}$ be measured with respect to the principal axes, so that the off-diagonal components are zero. Expanding and rearranging Equation (32) gives

$$h_1 = -t\,(S_{22}e_1 - S_{12}e_2)/(S_{11}S_{22} - S_{12}^2), \tag{33}$$

$$h_2 = -t\,(-S_{12}e_1 + S_{11}e_2)/(S_{11}S_{22} - S_{12}^2), \tag{34}$$

where matrix notation has been used (11 → 1 and 22 → 2). In the case of an isotropic surface,

$$h = -tYe, \tag{35}$$

where Y is the biaxial modulus equal to $1/(S_{11} + S_{12})$. Equations (33) and (34) were used to obtain interface stresses for crystalline polymers and n-paraffins (see Table 8). In the case of polyethylene, the interface stresses had a strong temperature dependence, presumably a result of significant entropic effects.

Ruud et al. [39,40] have determined interface stresses in an artificially multilayered thin film by measuring the amount of bending induced by the film in a much thicker substrate (see Table 9). It should be noted that the experimentally measured value for Ag(111)-Ni(111) is of opposite sign to that predicted theoretically (see Table 7). The reason for this major discrepancy is not clear. A similar study by Bain et al. [41] investigating strains in Mo(110)-Ni(111) multilayered films did not reveal any significant interface stresses. However, it has been suggested [39,40] that this was possibly due to intermixing between the layers.

TABLE 8. Experimental values of the interface stress $h_{ij}$ in materials that crystallize with a lamellar structure [35].

| Material | $h_{ij}$ [J/m$^2$] | Temperature [°C] |
|---|---|---|
| Melt-Crystallized Polyethylene | - 0.414, - 0.168 | 25 |
| n-Paraffins | - 0.472, - 0.364 | 23 |
| Random Copolymer of Tetrafluoroethylene and Hexafluoropropylene | - 0.2 | 300 |

TABLE 9. Experimentally measured interface stress h of multilayered thin films [39,40,42].

| Interface | h [J/m$^2$] |
|---|---|
| Au(111)/amorphous $Al_2O_3$ | 1.13 |
| Ag111)/Ni (111) | −2.27 |

Though the discussion so far has been limited to certain types of boundaries, interface stresses are associated with all types of solid-solid interfaces, such as grain boundaries and antiphase domain boundaries. One possible way to experimentally determine the interface stress of grain boundaries is by measuring the elastic strain it induces in a nanocrystalline material [see Equation (39)]. Cahn [43] has analyzed the critical behavior of the interfacial free energy and the interface stress of antiphase domain boundaries in ordered binary alloys with the B2 (β–CuZn) structure. An interface stress h will be present if the equilibrium lattice parameter is a function of the long range order parameter. Unlike the interfacial free energy σ, which is always positive, the interface stress h can be positive or negative. With respect to the critical behavior near the order-disorder transition temperature $T_c$, Cahn [43] showed that the classical (mean field) theory critical exponent for σ is 3/2 [that is, σ is proportional to $(T_c - T)^{3/2}$]. The critical exponent for σ according to modern critical theory is 1.3, while the exponents for h according to classical and modern critical theory are 1/2 and 0.0, respectively [43]. Thus, the magnitude of $h/\sigma$ tends to infinite as the critical point is approached.

## 4. Examples of Surface and Interface Stress Effects in Thin Films

In this section, recent investigations concerning the effects of surface and interface stresses on the structure and properties of thin films will be presented. Such stresses are often an important factor in determining thin film behavior because of the high surface area to volume ratio characteristic of these materials. It is shown that surface and interface stresses can result in a significant intrinsic stress, induce higher order elastic behavior, and affect the thermodynamics of epitaxy. Because of its similarity to the epitaxy problem, a discussion of surface reconstructions in (111) oriented fcc metal surfaces is also given.

### A. Strains and Elastic Modulus Variations in Ultrathin and Artificially Multilayered Films

Consider the in-plane elastic strains induced by the free surface stress f in a free-standing thin film of thickness t. The same type of analysis used to obtain Equation (35) would in this case lead to [44,45]

$$\varepsilon = -2f/Yt. \tag{36}$$

The factor of 2 accounts for the effects of both the top and bottom surfaces. Using typical values for metals of $f = 1\ J/m^2$ and $Y = 10^{11}\ J/m^3$ leads to an order of magnitude estimate

of the induced compressive in-plane strain of $\varepsilon = -0.02/t$, where t is measured in nm. Therefore, a 10 nm film would have an in-plane strain of about -0.2%, while a 2 nm thick film would have a strain of -1%. In principle, the surface stress can induce an elastic strain greatly in excess of the yield strain obtained by an externally applied stress. These large strains produce atomic displacements that are well out of the Hookean region of the interatomic potentials, so that higher order elastic effects should be manifested. Based on the theoretical calculations by Banerjea and Smith [46], the in-plane biaxial modulus of a Cu(100) disk depends on the in-plane strain in the following manner [44]:

$$Y(\varepsilon) = Y(0)\,[1 - B\varepsilon], \tag{37}$$

where B, which depends on the third order elastic constants, has a value of 15 to 25. Thus, a -1% strain in a Cu(100) free standing film would increase the apparent modulus by about 15 to 25%. A more complete analysis gives [19]

$$Y = Y_O + 2f(B + 2\eta - 3 + f'/f)/t \tag{38}$$

where $Y_O$ is the modulus value for a bulk material, $\eta$ is a factor that depends on Poisson's ratio and is close to unity, and f ' is equal to $\partial f/\partial\varepsilon$. Calculations of f ', which can be considered an "excess surface modulus," have shown that it can be negative [19,47,48]. For many (100) and (111) oriented fcc metal surfaces, the magnitude of $f'/f$ is significantly smaller than B [19], so that, according to Equation (38), the modulus should always be enhanced when t is reduced below about 5 nm.

Enhancements of nearly 50% in the biaxial modulus, as measured experimentally using a bulge test, were reported for free standing single crystal thin films of Au(100) when the thickness was reduced to about 100 nm [49]. If Equation (38) were used to explain this behavior, a surface stress of order 100 $J/m^2$ would be needed. Actually, the apparent enhancement is probably an experimental artifact. It has been shown [50,51] that erroneously large values by factors of 2 or more in the elastic modulus of thin films will be obtained from a thin film bulge test if the films are wrinkled. It is not easy to experimentally investigate free standing films with thicknesses less than 5 nm. It is however relatively easy to study them in a computer simulation. Elastic strains of order 1% and significant biaxial modulus enhancements were obtained in computer simulations of ultrathin films [19,52-54] that were in excellent agreement with Equations (36) and (38).

Although experimental measurements on ultrathin free standing films are problematical, similar lattice parameter changes [19,44,45] and modulus variations [19,44] are expected in artificially multilayered (superlattice) thin films owing to interface stress effects. In this case, Equations (36) and (38) would still apply, except that f and f ' should be

replaced with h and h', and t represents the bilayer repeat length. For systems with sufficiently large interface stresses, strains of order 1% proportional to 1/t, and modulus enhancements or reductions (depending on the sign of h) of order 20% are expected when the bilayer thicknesses are reduced below 5 nm. This behavior has in fact been observed experimentally [55]. The first experimental reports of modulus variations claimed enhancements of 100% or more (such enhancements were termed the "supermodulus effect"). However, the moduli were measured by the bulge test, and it is likely that the apparent modulus enhancements were artifacts of the measurement [50,51]. Recent measurements, using much more reliable ultrasonic methods, indicate that modulus variations involving both enhancements and reductions of order 20% are found for several multilayered metal films such as Cu-Nb [56]. Concomitant with these modulus variations are elastic strains proportional to 1/t that can be as large as a few percent. Though several theories have been proposed to explain this behavior, it has been most successfully modeled as a result of interface stress effects [19,44].

Large elastic strains and modulus variations would also be expected for other types of nanophase materials [35]. For example, in single component nanocrystalline metals and ceramics, if the grains are modeled as spheres, then, by analogy with Equation (17), there will be a strain dependence on the grain size d = 2r given by

$$\varepsilon = -4h/3Kd, \tag{39}$$

where h is the interface stress associated with the grain boundaries and K is the bulk modulus. Because of higher order elastic effects induced by this strain, the bulk modulus will depend on d [57]:

$$K(d) = K_0 + 4h\,(B_b - 1 + h'/h)/3d, \tag{40}$$

where $K_0$ is the bulk modulus for a bulk material and $B_b$ is the factor for the bulk modulus that is analogous to the factor B for the biaxial modulus in Equation (37). Other properties that depend on elastic strain should also be affected by interface stress effects. For example, since the oscillatory nature of the Ruderman-Kittel-Kasuya-Yosida (RKKY) interaction is strongly affected by changes in the interatomic distance, interface stress effects in nanocrystalline materials could result in novel magnetic behavior.

**B. Intrinsic Stress**

Almost all thin films are deposited in a state of stress. These stresses develop because certain processes occur which would result in the film changing its in-plane dimensions if it were not attached to the substrate [58]. A well known example is thermal

stress which develops in response to a change in temperature when the thermal expansion coefficients of the film and substrate are different. Intrinsic stresses are defined as those stresses that develop during film growth. Various mechanisms for intrinsic stress generation have been proposed [58]. One possibility that has often been mentioned, though it has been little investigated, is intrinsic stress generation due to effects of the free surface stress f. (Many workers refer to this idea as based on "crystal size effects.") There appears to be some confusion in the literature as to the precise formulation of this effect, its relative importance, and even the sign of the intrinsic stresses that are developed. Because of this a relatively detailed discussion is presented below.

Consider an isotropic film of thickness t that is constrained to have its bulk lattice parameter. Assume that there is not a strong film-substrate interaction so that $f >> g$. Suppose that when the constraint is removed, the film elastically deforms on the substrate in response to the surface stress f. Letting $\varepsilon$ represent the resultant elastic in-plane radial strain, the elastic energy per unit area in the film is given by $Yt\varepsilon^2$, where Y is the biaxial modulus equal to $E/(1 - \nu)$, where E is Young's modulus and $\nu$ is Poisson's ratio. The work per unit area performed against the surface stress can be expressed as $2f\varepsilon$. The total work per unit area is therefore

$$w = 2f\varepsilon + Yt\varepsilon^2. \tag{41}$$

The equilibrium strain $\varepsilon^*$ is determined by setting $\partial w/\partial \varepsilon = 0$:

$$\varepsilon^*(t) = -f/Yt\,. \tag{42}$$

Based on this result, it has been sometimes argued that the intrinsic stress resulting from opposing this deformation would equal $-Y\varepsilon^*(t)$, and therefore should be of the same sign as f and be inversely proportional to t. However, this is not the correct physical picture with regard to generating an intrinsic stress in a film. A film on a substrate that displays an equilibrium strain relative to bulk does not have to be under a state of intrinsic stress. Instead, if at some point during deposition the film is firmly attached to the substrate, an intrinsic stress will subsequently be generated by the surface stress as the film thickness increases.

This idea can be made quantitative in the following manner. Consider a film that has become firmly attached to the substrate at a thickness $t_o$. Assuming no intrinsic stress generating mechanisms have operated, the film would be deposited in a stress-free state with its equilibrium in-plane lattice parameter equal to $a_o[1 + \varepsilon^*(t_o)]$, where $a_o$ is the bulk lattice parameter. During further deposition, if the film were not constrained by the substrate, the equilibrium strain relative to bulk $\varepsilon^*(t)$ would be given by Equation (42), and

the equilibrium strain relative to that of the film of thickness $t_o$ would be $\Delta\varepsilon = \varepsilon^*(t) - \varepsilon^*(t_o)$. However, since the film of thickness $t_o$ was constrained by the substrate such that it could not elastically deform in the plane of the film, then as the film becomes thicker, the substrate must impose an in-plane biaxial stress to oppose the latent strain $\Delta\varepsilon$. As a result, an intrinsic stress s is generated in the film due to surface stress effects equal to

$$s(t) = -Y\Delta\varepsilon = f\,(1/t - 1/t_o). \tag{43}$$

As $t \rightarrow \infty$, the intrinsic stress approaches a value of $s = -f/t_o$. Even though the above analysis considered just the effects of the surface stress, and it was assumed that the film of thickness $t_o$ was stress-free, the result given in Equation (43) is nevertheless of general validity. That is, Equation (43) represents the contribution to the overall intrinsic stress of the film resulting from the surface stress, independent of other stress generating mechanisms (and even if the lattice parameter is different from $a_o[1 + \varepsilon^*(t_o)]$ when the film thickness is $t_o$).

Consideration is now given to the proper value of the film thickness $t_o$. It would appear plausible that growing crystallites first become constrained when substantial impingement occurs. The thickness at which this occurs would depend in part on the thermodynamics of the film-substrate interface; in particular, it would depend on how well the film wets the substrate. The thickness $t_o$ would also be dependent in large part on kinetic factors, such as the deposition rate and the surface mobility of the adatoms (which in turn depends on the deposition temperature). Experimental studies have indicated that a metal film deposited by physical vapor deposition can become continuous at a thickness as small as 1 nm [59]. Referring to Equation (43), and using reasonable values of $f = 2$ N/m and $t_o = 5$ nm, the magnitude of the intrinsic stress generated when $t >> t_o$ is of order $-4 \times 10^8$ Pa. It should be noted that the intrinsic stress has the opposite sign of the surface stress.

Since most experimental and theoretical investigations of surface stresses for metals give positive values, the proposed mechanism would be expected to produce a compressive intrinsic stress in metallic films. It is generally found that at the end of nonepitaxial growth, metallic films exhibit a tensile intrinsic stress. However, it is often observed during the early stages of deposition that the film is initially deposited with a compressive stress which increases in magnitude with increasing thickness, up to a certain thickness, after which a competing tensile stress generating mechanism appears and eventually dominates. Two popular models to explain generation of a tensile stress in metal films are the grain growth model and the grain boundary relaxation model [58]. In both processes the total grain boundary volume reduces with time. This reduction would lead to a densification of the film were it not constrained by the substrate. Kinetic analyses

of these processes have been given by Doerner and Nix [58]. They showed that in both cases a significant amount of time can elapse before a perceptible tensile stress is developed. During this time the film can grow to a thickness many times larger than $t_o$. As a result, a compressive intrinsic stress due to the surface stress can develop before the other processes generate a competing tensile stress that eventually dominates. (Of course, for some thin films the surface stress could be negative; in those cases, the intrinsic stress generated by the surface stress would be tensile.)

In the above discussion, the effect of the film-substrate interface stress was not considered. If there is a strong epitaxial relationship between a film and substrate, this interface stress g could of course be very important and in fact dominate the behavior. However, if there is not a strong epitaxial relationship (for example, metal deposition on an amorphous substrate), then the interface stress is expected to be much less important. In either case, the effect of the film-substrate interface stress can be formally taken into account by considering f to be a net surface stress equal to the sum of the free surface stress and the film-substrate interface stress. If the film is polycrystalline, the interface stress h of the grain boundaries could contribute a term to the intrinsic stress. In the case of films with a columnar microstructure, this term will depend on grain size and not on film thickness [57]. As a result, the grain boundary interface stress will not play a role in intrinsic stress development until significant grain growth occurs, and it is therefore not expected to be important during the early stages of deposition.

### C. Thermodynamics of Epitaxy

When an epitaxial film is deposited by a layer-by-layer growth process onto a thick substrate that has a lattice parameter different from that of the film, the misfit strain can be accommodated by straining the film in order to bring it into partial or complete registry with the substrate and/or by generating misfit dislocations at the film-substrate interface. If this misfit strain is not too large, there is a critical film thickness below which the equilibrium film–substrate interface is coherent, and above which it is thermodynamically favorable for some of the misfit to be accommodated by interfacial dislocations.

A simple model [60] for the critical thickness for epitaxy will now be presented that is based on one given by Matthews [34], except that it is extended to include surface stress effects. Let $\varepsilon$ be the uniform radial strain in the film relative to its bulk equilibrium state. Three separate work terms can be considered: the volume elastic energy, the work associated with changing the defect structure at the film-substrate interface, and the work to stretch the film surface. The elastic energy per unit area can be expressed as $Yt\varepsilon^2$. According to Equation (28), the change in the film-substrate interface energy per unit area can be expressed as $2(g - \sigma_o)\varepsilon$. The work per unit area to stretch the film surface can be expressed as $2\,\partial\gamma/\partial\varepsilon\;\varepsilon = 2(f - \gamma)\varepsilon$. (This term was incorrectly given as $2f\varepsilon$ in reference 60).

The factors of 2 in the second and third terms reflect the two-dimensional nature of the planar strain. The total work per unit area can be expressed as

$$w = Yt\varepsilon^2 + 2(g - \sigma_o)\varepsilon + 2(f - \gamma)\varepsilon. \tag{44}$$

Most analyses of the thermodynamics of epitaxy only consider effects of the first two terms on the right hand side of Equation (44). Such analyses are incomplete as they ignore the effects of the free surface stress which can be significant. The equilibrium strain $\varepsilon^*$ can be determined by minimizing w with respect to $\varepsilon$:

$$\varepsilon^* = -(f + g - \gamma - \sigma_o)/Yt. \tag{45}$$

The critical thickness can be obtained by setting $\varepsilon^*$ equal to the misfit strain $\varepsilon_m$:

$$t_c = -(f + g - \gamma - \sigma_o)/Y\varepsilon_m. \tag{46}$$

Figure 4 gives plots of the critical thickness for epitaxy as a function of the magnitude of the misfit strain. The parameters g and $\sigma_o$ were calculated using Equations (26) and (27) and employing typical values for metals and semiconductors for the shear constants and the Burgers vector. The difference between the surface stress and surface free energy was taken to be $f - \gamma = 2\,J/m^2$. Curve (a) is for $\varepsilon_m > 0$, and curve (c) is for $\varepsilon_m < 0$. Curve (b) was obtained by setting $f = \gamma$; it is representative of previous models that have ignored the effects of the surface stress. Comparison of curves (a) and (c) shows that at the

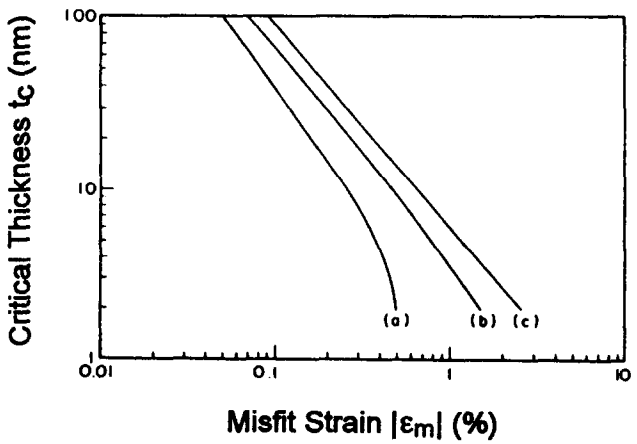


Figure 4. Critical thickness for epitaxy as a function of misfit strain [60].
(a) $f - \gamma = 2\,J/m^2$, $\varepsilon_m > 0$; (b) $f - \gamma = 0$; (c) $f - \gamma = 2\,J/m^2$, $\varepsilon_m < 0$.

larger magnitude misfits, inclusion of the surface stress term in the analysis can change the critical thickness by almost an order of magnitude when the sign of the misfit strain is changed.

### D. Surface Reconstructions of Clean Metal Surfaces

Recently, it has been found that clean (111) oriented Pt surfaces reconstruct above 0.65 $T_m$, where $T_m$ is the melting temperature [61]. The reconstruction can be described as a continuous commensurate-incommensurate transformation in which the surface layer is isotropically compressed relative to the underlying bulk lattice. A similar reconstruction occurring above 0.65 $T_m$ has also been reported for (111) oriented Au surfaces [62]. At lower temperatures, a 23 x $\sqrt{3}$ reconstruction has been observed in Au(111) that can be described as an insertion of an extra row of atoms every 23 rows on the surface [63]. This one-dimensional relaxation represents a surface compression of about 4%. All other clean (111) fcc metal surfaces studied (Ir, Al, Ni, etc.) have not displayed a surface reconstruction.

A theory for surface reconstruction of fcc metal surfaces using the Frenkel-Kontorova model for a one-dimensional surface was proposed by Needs et al. [9]. The surface was modeled as a linear array of atoms connected by springs, and the atoms sat in a sinusoidal potential that represented the underlying lattice. The stability of the surface was characterized by a parameter P which, for the case of a (100) oriented surface of a simple cubic metal, was given by [9]

$$P = \pi a(f - \gamma)/2(2kW)^{1/2}, \tag{47}$$

where a is the lattice parameter, f and $\gamma$ are the surface stress and surface free energy of the unreconstructed surface, k is a spring constant associated with surface bonds, and W is the peak- to- peak amplitude of the sinusoidal surface-substrate interaction potential. If $|P| < 1$, an unreconstructed surface is stable; otherwise, a surface reconstruction is expected. This model was applied with appropriate modifications to (111) oriented surfaces of Au, Pt, Ir, and Al. Although it was expected that accurate values for f and $\gamma$ could be obtained from their first principles calculations, Needs et al. found that values for k and especially for W could only be crudely estimated. Their results suggested that all of the metals, including Au and Pt, should be stable to reconstruction. The lack of agreement with experimental observation was attributed to the uncertainty concerning k and especially W. Nevertheless, the model clearly demonstrated that although there may be a driving force for reconstruction, the energy cost associated with the loss of structural coherence of the surface with the underlying bulk is generally too large to make the structural transition thermodynamically favorable.

Herring [3] proposed a continuum model to analyze this type of surface reconstruction that was recently rederived and extended [64]. Consideration will be given first to the one-dimensional compression associated with the low temperature surface reconstruction of Au(111). As with the epitaxy model, there are three terms whose sum represents the work per unit area needed to introduce an elastic strain in the top monolayer. First, there is a term that takes into account the elastic energy of the surface layer that is strained by an amount $\varepsilon < 0$ in one direction, but is constrained not to deform in the perpendicular in-plane direction. This elastic energy can be expressed as $E\varepsilon^2 t/2(1-\nu^2)$, where t is the surface layer thickness. The second term is associated with the energy of the noncoherent interface between the strained surface atoms and the underlying lattice. This term can be taken as the energy needed to form a periodic row of "surface" edge dislocations that accommodates the in-plane misfit strain $\varepsilon$ and can be expressed [64] as $\alpha Gb|\varepsilon| = -\alpha Gb\varepsilon$, where G is the shear modulus and $\alpha \approx [4\pi(1-\nu)]^{-1}$, where $\nu$ is Poisson's ratio. Lastly, there is a term associated with the change in the surface free energy owing to the elastic strain $\varepsilon$ and concomitant change in the surface density of atoms which can be expressed as $(f-\gamma)\varepsilon$. The total work associated with the transformation from a structurally coherent surface to a relaxed surface of unit area can be written as

$$w = Et\varepsilon^2/2(1-\nu^2) - \alpha Gb\varepsilon + (f-\gamma)\varepsilon. \tag{48}$$

An instability criterion can be established by setting $w < 0$. Restricting attention to the onset of the reconstruction transition ($\varepsilon \rightarrow 0$) leads to the following condition for the surface to be unstable [3,64]:

$$(f-\gamma)/Gb > \alpha. \tag{49}$$

The parameter $\beta \equiv (f-\gamma)/Gb$ can be interpreted as the change in energy per unit elastic strain of the surface divided by an elastic energy related to the formation of a dislocation. When $\beta$ is less than the critical value $\alpha \approx 0.1$, the unreconstructed surface is stable. If $\beta$ exceeds the critical value, the surface is predicted to reconstruct.

The above analysis applies to a surface reconstruction associated with a one-dimensional compression. The total work associated with a two-dimensional compression can be expressed as

$$w = Yt\varepsilon^2 - 2\alpha Gb\varepsilon + 2(f-\gamma)\varepsilon, \tag{50}$$

where Y is the biaxial modulus, and the factors of 2 reflect the two-dimensional nature of the total strain. This equation is essentially equivalent to Equation (44) with the misfit

strain $\varepsilon_m$ set equal to zero. It should be noted that setting $w < 0$ for $\varepsilon \rightarrow 0$ leads to the same stability criterion as for the one-dimensional case.

The instability criterion developed above will now be compared to experimental observation. Consideration is first given to the set of metals considered by Needs and coworkers: Al, Ir, Pt, and Au. The parameter $\beta$ was computed [64] for each surface using the values of the surface free energy and the surface stress given in Table 1, and is given in Table 10. As can be seen, the criterion $\beta > 0.1$ correctly predicts which metals have been observed to display a surface reconstruction (Au and Pt). Although Au and Ir have about the same driving force for surface reconstruction, equal to $(f - \gamma)$, Ir has a shear modulus almost an order of magnitude larger than that of Au. As a result, the opposing force for reconstruction, the energy to create a noncoherent interface, is large enough to keep the unreconstructed surface of Ir stable but small enough to allow Au to reconstruct. The same calculation for $\beta$ was also performed for Pb and is given in Table 10. Since $\beta$ exceeds the critical value of 0.1 and is close to that for Au and Pt, the model predicts that the clean Pb(111) surface should reconstruct [64]. This surface has not been studied in detail, so it is not known if it displays the predicted reconstruction.

TABLE 10. Calculated values for the stability parameter $\beta$ for clean (111) fcc metal surfaces [64].

| Metal | $\beta$ |
|---|---|
| Al | 0.041 |
| Ir | 0.034 |
| Pt | 0.19 |
| Au | 0.19 |
| Pb | 0.17 |

It is possible to derive from the continuum model an expression for the equilibrium amount of elastic strain associated with the reconstruction. This can be obtained by setting $\partial w/\partial \varepsilon = 0$. From Equation (48) the equilibrium strain for the one-dimensional compression is

$$\varepsilon = (\alpha G b + \gamma - f)(1 - \nu^2)/Et. \tag{51}$$

Using Equation (51), a calculation for the strain in the low temperature reconstruction of Au gives $\varepsilon = -3\%$. This can be considered in reasonable agreement with the experimental

value of $-4\%$. For the case of the two-dimensional compression associated with the high temperature reconstructions, the equilibrium strain would be

$$\varepsilon = (\alpha Gb + \gamma - f)/Yt. \tag{52}$$

The fact that experimentally the strain appears to vary continuously for the high temperature reconstructions of Au(111) and Pt(111) may indicate a significant dependence of f and $\gamma$ on temperature.

Other metal surface reconstructions may be attributable to surface stress effects. For example, it appears that it is thermodynamically favorable for several clean (100) oriented fcc metal surfaces to reconstruct by having the top layer of atoms transform from a square lattice arrangement to a hexagonal (111)-type arrangement due to the reduction in surface free energy [64]. However, this type of reconstruction has only been observed for a few metals (Au, Pt, Ir). Interestingly, the inequality $(f - \gamma)/Gb > \alpha$ appears to successfully predict which (100) oriented surfaces will reconstruct in this manner [64]. One possible reason for this is that surface stress effects may enhance the kinetics of the transformation by allowing the (100) surface to overcome an activation barrier by first transforming to an intermediate state in which the ideal 1 x 1 surface experiences an in-plane compression.

Based on a suggestion by Orowan [65], Andreussi and Gurtin [66] developed a continuum model to describe the "buckling" (or "wrinkling") of a free surface due to surface stress effects. They showed that when the sum of the surface stress f and the "surface modulus" f ' is less than zero, there is a driving force for the surface to buckle. The predicted wavelength and amplitude of the buckling was found to be of order 0.1 nm when $f + f'$ was of order $-1\ J/m^2$. As pointed out by Dregia et al. [48], this model can be used to explain the 2 x 1 reconstruction of Au(110) and Pt(110). The reconstructed surface can be described as having a "missing row" structure which results from removing every other row of atoms from the top monolayer. Computer simulations using embedded atom potentials performed by Dregia et al. [48] indicated that $f + f'$ is less than zero for the (110) oriented surfaces of Au and Pt, and the predicted periodicity of the buckling was close to the value of two interatomic distances characteristic of the missing row reconstruction. Interestingly, a similar buckling of Au(111) surfaces was observed by Marks et al. [67] using high resolution electron microscopy, except that the wavelength and amplitude of the buckling were several atomic spacings.

It has recently been suggested [68] that every surface for which $f \neq \gamma$ should display a reconstruction of the type discussed for (111) oriented surfaces of Au and Pt. However, it is only correct to say that when $f \neq \gamma$, there is a driving force for reconstruction. In most cases the opposing force, which is the energy cost associated with the top monolayer losing structural coherence with the underlying lattice, is too large to make the reconstruction

thermodynamically favorable [9,64,69,70]. Except for the examples cited above, it is not clear what role if any the surface stress plays in other types of reconstructions. Unlike metals, where most low index 1 x 1 surfaces are stable, many semiconductor surfaces display a reconstruction. This suggests that the driving forces for reconstructions observed in semiconductors are different from those for metals. In the case of Si(111), Vanderbilt [71] has shown that the 7 x 7 structure is more stable than the ideal 1 x 1 because of dangling bond reductions despite surface stress effects that oppose the reconstruction.

## Acknowledgments

The author thanks S.M. Prokes, K. Sieradzki, D. Vanderbilt, J.W. Cahn, A.L. Greer, S.A. Dregia, F. Spaepen, F.H. Streitz, J.A. Ruud, R.K. Eby, and M.R. Scanlon for stimulating discussions, and J.B. Savader, T.M. Trimble, N.A. Vaught, and R.W. Cammarata for critical readings of the manuscript. This work was supported in part by the National Science Foundation under grant no. ECS-920222 and the Office of Naval Research under grant number N00014-91-J-1169.

## References

1. J.W. Gibbs, *The Scientific Papers of J. Willard Gibbs*, Vol. 1 (Longmans-Green, London, 1906) p. 55.

2. R. Shuttleworth, *Proc. Phys. Soc.* **A63**, 445 (1950).

3. C. Herring, in *The Physics of Powder Metallurgy*, W.E. Kingston, ed. (McGraw-Hill, New York, 1951) p.143.

4. H. Brooks, in *Metal Interfaces* (American Society for Metals, Metals Park, Ohio, 1963) p. 20

5. C. Herring, in *Structure and Properties of Solid Surfaces*, R. Gomer and C.S. Smith, eds. (University of Chicago, Chicago, 1953) p. 5.

6. W.W. Mullins, in *Metal Surfaces: Structure, Kinetics and Energetics* (American Society for Metals, Metals Park, Ohio, 1963) p. 17.

7. J.W. Cahn, in *Interfacial Segregation*, W.C. Johnson and J.M. Blakely, eds. (American Society for Metals, Metals Park, Ohio, 1979) p. 3.

8. A.J. Shaler, in *Structure and Properties of Solid Surfaces*, R. Gomer and C.S. Smith, eds. (University of Chicago, Chicago, 1953) p. 5

9. R.J. Needs, M.J. Godfrey, and M. Mansfield, *Surf. Sci.* **242**, 215 (1991).

10. J.W. Cahn, *Acta Metall.* **28**, 1333 (1980).

11. D.M. Heyes, *J. Chem. Phys.* **79**, 4010 (1983).

12. R.J. Needs and M. Mansfield, *J. Phys. (Condensed Matter)* **1**, 7555 (1989).

13. R.J. Needs and M.J. Godfrey, *Phys. Rev. B* **42**, 10933 (1990).

14. M. Mansfield and R.J. Needs, *Phys. Rev. B* **43**, 8829 (1991).

15. P. Gumbsch and M. Daw, *Phys. Rev. B* **44**, 3934 (1991).

16. D. Wolf, *Surf. Sci.* **236**, 389 (1990).

17. G.J. Ackland and M.W. Finnis, *Phil. Mag* A **54**, 301 (1986).

18. G.J. Ackland, G. Tichy, V. Vitek, and M.W. Finnis, *Phil. Mag.* A **56**, 735 (1987).

19. F.H. Streitz, R.C. Cammarata, and K. Sieradzki, submitted to *Phys. Rev. B*.

20. R.D. Meade and D. Vanderbilt, *Phys. Rev. B* **40**, 3905 (1989).

21. R.D. Meade and D. Vanderbilt, *Phys. Rev. Lett.* **63**, 1404 (1989).

22. J.W. Cahn and R. E. Hanneman, *Surf. Sci.* **1**, 387 (1964).

23. M.M. Nicholson, *Proc. Roy. Soc.* A **228**, 490 (1955).

24. G.C. Benson and K.S. Yun, *J. Chem. Phys.* **42**, 3805 (1965).

25. S.N. Zadumkin and A. I. Temrokov, *J. Sov. Phys.* **11**, 35 (1968).

26. C.W. Mays, J.S. Vermaak, and D. Kuhlmann-Wilsdorf, *Surf. Sci.* **12**, 134 (1968).

27. H.J. Wassermann and J.S. Vermaak, *Surf. Sci.* **22**, 164 (1970).

28. H.J. Wassermann and J.S. Vermaak, *Surf. Sci.* **32**, 168 (1972).

29. M. Ohring, *The Materials Science of Thin Films* (Academic, Boston, 1992) p. 413.

30. R.E. Hanneman, M.C. Finn, and H.C. Gatos, *J. Phys. Chem. Solids* **23**, 1553 (1962).

31. R.E. Martinez, W.M. Augustyniak, and J.A. Golovchenko, *Phys. Rev. Lett.* **64**, 1035 (1990).

31a. A.J. Schell-Sorokin and R.M. Tromp, *Phys. Rev. Lett.* **64**, 1039 (1990).

31b. R.D. Meade and D. Vanderbilt, in *Springer Series in Surface Sciences, Vol. 24: The Structure of Surfaces III*, S.Y. Tong, M.A. Van Hove, and X.D. Xie, eds. (Springer-Verlag Berlin, Heidelberg, 1991) p. 4

32. S. Lehwald, F. Wolf, H. Ibach, B.M. Hall, and D.L. Mills, *Surf. Sci.* **192**, 131 (1987).

33. J.W. Cahn and F. Larché, *Acta. Metall.* **30**, 51 (1982).

34. J.W. Matthews, in *Epitaxial Growth*, J.W. Matthews, ed. (Academic, New York, 1975) p. 559

35. R.C. Cammarata and R.K. Eby, *J. Mater. Res.* **6**, 888 (1991).

36. G.T. Davis, R.K. Eby, and J.P. Colson, *J. Appl. Phys.* **41**, 4316 (1970).

37. G.T. Davis, J.J. Weeks, G.M. Martin, and R.K. Eby, *J. Appl. Phys.* **45**, 4175 (1974).

38. I.C. Sanchez, J.P. Colson, and R.K. Eby, *J. Appl. Phys.* **44**, 4332 (1973).

39. J.A. Ruud, A. Witrvrouw, and F. Spaepen, *Mater. Res. Soc. Symp. Proc.* **209**, 737 (1991).

40. J.A. Ruud, A. Witrvrouw, and F. Spaepen, *J. Appl. Phys.* **74**, 2517 (1993).

41. J.A. Bain, L.J. Chyung, S. Brennan, and B.M. Clemens, *Phys. Rev. B* **44**, 1184 (1991).

42. J.A. Ruud, Ph.D. Thesis, Harvard University (1992).

43. J.W. Cahn, *Acta Metall.* **37**, 713 (1986).

44. R.C. Cammarata and K. Sieradzki, *Phys. Rev. Lett.* **62**, 2005 (1989).

45. Yu.A. Kosevich and A.M. Kosevich, *Solid State Comm.* **70**, 541 (1989).

46. A. Banerjea and J.R. Smith, *Phys. Rev. B* **35**, 5413 (1987).

47. C.W. Price and J.P. Hirth, *Surf. Sci.* **57**, 509 (1976).

48. S.A. Dregia, C.L. Bauer, and P. Wynblatt, *J. Vac. Sci. Technol.* A **5**, 766 (1987).

49. A. Catlin and W.P. Walker, *J. Appl. Phys.* **31**, 2135 (1960).

50. H. Itozaki, Ph.D. Thesis, Northwestern University (1982).

51. S.P. Baker, M.K. Small, J.J. Vlassak, B.J. Daniels, and W.D. Nix, in *Mechanical . Properties and Deformation Behavior of Materials Having UltrafineMicrostructures*, M. Nastasi, D.M. Parkin, and H. Gleiter, eds. (Kluwer Academic, Dordrecht, 1993) p. 165.

52. D. Wolf and J.F. Lutsko, *Phys. Rev. Lett.* **60**, 1170 (1988).

53. B.W. Dodson, Phys. *Rev. Lett.* **60**, 2288 (1988).

54. F.H. Streitz, R.C. Cammarata, and K. Sieradzki, *Phys. Rev. B* **41**, 12285 (1990).

55. For a recent review, see R.C. Cammarata, in *Mechanical Properties and Deformation Behavior of Materials Having Ultrafine Microstructures*, M. Nastasi, D.M. Parkin, and H. Gleiter, eds. (Kluwer Academic, Dordrecht, 1993) p. 193.

56. A. Fartash, E.E. Fullerton, I.K. Schuller, S.E. Bobbin, J.W. Wagner, R.C. Cammarata, S. Kumar, and M. Grimsditch, *Phys. Rev. B* **44**, 13760 (1991).

57. R.C. Cammarata, to be published.

58. M.F. Doerner and W.D. Nix, CRC *Critical Reviews in Solid State and Materials Science* **14**, 244 (1988).

59. R.F. Bunshah, in *Deposition Technologies for Films and Coatings*, R.F. Bunshah, ed. (Noyes, Park Ridge, New Jersey, 1982) p. 83.

60. R.C. Cammarata and K. Sieradzki, Appl. *Phys. Lett.* **55**, 1197 (1989).

61. A.R. Sandy, S.G.J. Mochrie, D.M. Zehner, G. Grubel, K.G. Huang, and D. Gibbs, *Phys. Rev. Lett.* **68**, 2192 (1992).

62. K.G. Huang, D. Gibbs, D.M. Zehner, and S.G. J. Mochrie, *Phys. Rev. Lett.* **65**, 3313 (1990).

63. U. Harten, A.M. Lahee, J.P. Toennies, and Ch. Woll, *Phys. Rev. Lett.* **54**, 2619 (1985).

64. R.C. Cammarata, *Surf. Sci.* **279**, 341 (1992).

65. E. Orowan, *Proc. R.oy Soc.* A **316**, 473 (1970).

66. F. Andreussi and M.E. Gurtin, *J. Appl. Phys.* **48**, 3798 (1977).

67. L.D. Marks, V. Heine, and D.J. Smith, *Phys. Rev. Lett.* **52**, 656 (1984).

68. D. Wolf, *Phys. Rev. Lett.* **70**, 627 (1993).

69. R.J. Needs, *Phys. Rev. Lett.* **71**, 460 (1993).

70. M.Y. Chou, S. Wei, and D. Vanderbilt, *Phys. Rev. Lett.* **71**, 461 (1993).

71. D. Vanderbilt, *Phys. Rev. Lett.* **59**, 1456 (1987).